



Generation and probing of 3D helical lattices with tunable helix pitch and interface

ZHIWEI SHI,^{1,2,3} DARYL PREECE,⁴ CHENSONG ZHANG,² YINXIAO XIANG,²
AND ZHIGANG CHEN^{2,5,*}

¹*School of Electro-mechanical Engineering, Guangdong University of Technology, Guangzhou 510006, China*

²*Department of Physics & Astronomy, San Francisco State University, San Francisco, CA 94132, USA*

³*Guangdong Provincial Key Laboratory of Nanophotonic Functional Materials and Devices, School of Information and Optoelectronic Science and Engineering, South China Normal University, Guangzhou 510006, China*

⁴*Department of Biomedical Engineering, University of California Irvine, Irvine, CA, USA*

⁵*The MOE Key Laboratory of Weak-Light Nonlinear Photonics, TEDA Applied Physics Institute and Physics of School, Nankai University, Tianjin 300457, China*

*zhigang@sfsu.edu

Abstract: We propose a method for generation of tunable three-dimensional (3D) helical lattices with varying helix pitch. In order to change only the lattice helix pitch, a periodically varying phase along the propagation direction is added to the central beam – one of the interference beams for lattice construction. The phase periodicity determines the helix pitch, which can be reconfigured at ease. Furthermore, a helical lattice structure with an interface (domain wall) is also achieved by changing the phase structure of the lateral beams, leading to opposite rotating direction (helicity) on different sides of the interface. When a Gaussian beam is used to probe the bulk lattice, it can evolve into a spiral beam with its helicity varying in accordance with that of the lattice. Probing along the interface with two dipole-like optical beams leads to unusual propagation dynamics, depending on the phase and size of the two beams. This approach could be further explored for studies of nonlinear interface solitons and topological interface states. In addition, the helical lattices may find applications in dynamical multi-beam optical tweezers.

© 2019 Optical Society of America under the terms of the [OSA Open Access Publishing Agreement](#)

1. Introduction

In optics, periodic or quasiperiodic waveguide arrays are associated with materials that exhibit a refractive index modulation in one or more spatial dimensions. They can significantly modify the overall optical properties of the materials as well as strongly affect the propagation of light [1–25]. Naturally, an optical beam propagates along a straight line, but synthetic photonic structures can support rotational propagation which incorporates more interesting dynamics and applications not found in free space or homogenous media [12–24]. For instance, a rotating waveguide array can support localized (bulk or edge) modes existing even in the linear region, in sharp contrast to localized states in nonrotating arrays that typically require a defect or a nonlinearity [17]. In an array of evanescently coupled helical waveguides arranged in a graphene-like honeycomb lattice, one-way edge states that are topologically protected from back-scattering have been demonstrated [20], driving the active field of topological photonics [21]. Indeed, the helical honeycomb photonic lattices could be a useful platform to investigate a number of fundamental phenomena such as nonlinear topological edge solitons [22,23], anomalous topological phases [24], and photonic topological valley Hall edge states [25].

To create helical waveguides in experiments, one can directly write them into fused silica glass using a femtosecond laser [18,25], or use the optical induction in a nonlinear crystal [16,26]. The latter approach has been shown to provide a highly flexible and convenient way

to fabricate many different linear and nonlinear optical lattices [3,4]. Generation of helical beams (HBs) in free space has also been investigated, and the most common method for creating such HBs has been relied on the use of a forked hologram. When the hologram is illuminated with a plane wave, the first-order diffracted beams exhibit helical phase structure [27]. The inverted Gabor holography principle for tailoring arbitrary shaped 3D beams including HBs has also been studied numerically and experimentally [28]. Another typical example is the so-called optical solenoid beams, which come from the solutions of the Helmholtz equation as a particular superposition of m -th order Bessel beams, propagating without diffraction with their principal intensity maximum spiraling around the optical axis [29]. Other alternative methods are proposed and developed based on a superposition of multiple coherent waves by using interferometric schemes [30–36], spatial light modulators [35,36], pinhole arrangements [30,37], colloidal monolayers of dielectric microparticles [38], or the Talbot effect [39,40].

In most of these studies which use the multi-beam interference, so far the attention has been focused on the generation of photonic lattices with different transverse shapes (triangular, quadratic, hexagonal or the like), or the formation of corresponding helical lattices (HLs) [26,30–37]. The issue of how to control the helix pitch and the spiral direction, both important for optical functionalities of HLs [17,20,22,24], have not been fully addressed. In this work, we discuss the generation of photonic HLs with controllable helix pitch and helical rotation direction based on fine-tuning the parameters in multi-beam interference. In particular, we propose a simple method to create an interface between two helical waveguide arrays with same or opposite helicities, much desired in the study of edge states and topological phenomena.

2. Theoretical description of multi-beam interference

The multi-beam interference model involves an optical pattern formed by the superposition of multiple non-coplanar beams. The beam pattern depends on the number of beams and their associated configuration [33]. Formed by the interference of N monochromatic noncoplanar plane waves, the time-averaged intensity distribution of the pattern can be expressed as [23,27–32]

$$I(\vec{r}) = \frac{1}{2} \sum_{i=1}^N E_i^2 + \sum_{j>i}^N V_{ij} \cos((\vec{k}_i - \vec{k}_j) \cdot \vec{r} + \delta\phi_{ij}), \quad i, j = 1, 2, 3 \dots N, \quad (1)$$

where V_{ij} is the interference coefficient defined by $V_{ij} = E_i E_j (\vec{e}_i \cdot \vec{e}_j)$. The i th plane wave at the point $\vec{r}(x, y, z)$ in a sample plane x - y at a time t may be presented by $E_i(\vec{r}) = E_i \cos(\vec{k}_i \cdot \vec{r} + \phi_i - \omega t) \vec{e}_i$, where E_i is the amplitude, ω is the frequency, \vec{k}_i is the wavevector, $\delta\phi_{ij} = \phi_i - \phi_j$ is the phase difference, and \vec{e}_i denotes the polarization vector.

As shown in Fig. 1, we assume that there are seven beams k_i ($i=1,2,\dots,7$) whose wavelengths are all set at $\lambda = 488\text{nm}$ - the one typically used for photorefractive induction of photonic lattices [1–4]. The central beam k_7 is along the optical axis (z axis) while the side beams k_i ($i=1,2,\dots,6$) are arranged symmetrically around k_7 at an angle θ from z axis forming an umbrella-like structure. If we do not consider the central beam k_7 , the side beams will only form the 2D hexagonal lattice as shown in Fig. 2 (b) at $z = 0$. When we include k_7 as a different wave vector component in the direction of the optical axis into the interference with other plane waves, the phase singularities of the vortices are effectively transformed into the desired helical intensity structure [26,30]. In this case, 3D hexagonal helical lattices can be established based on the interference of seven beams. In addition, a phase shift may be introduced by elliptical polarization in one or more of the interfering beams to produce

compound lattices [30]. Here, we assume that k_7 is circularly polarized while the other six beams are linearly polarized for simplicity. In general, strontium barium niobate (SBN) crystal has been used for the fabrication of optical induction lattices, so we have used the refractive index of the medium as $n = 2.3$ in our numerical simulation. The required beam structures or lattice structures are decided by the parameters of the beam, we discuss how to achieve novel lattice structures by controlling the beam parameters in the following sections.

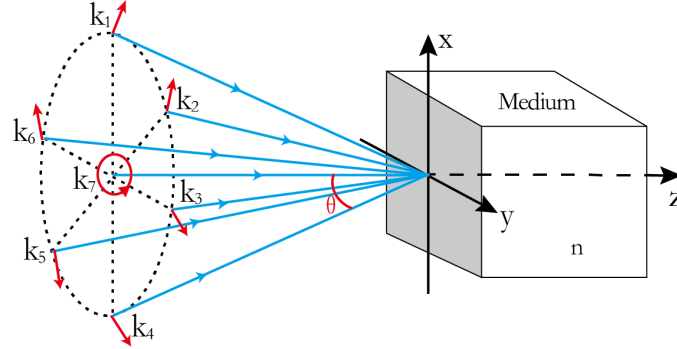


Fig. 1. Schematic of interference configuration of seven beams for optical induction of HLs in a nonlinear crystal, where k_i ($i=1,2,\dots,7$) denotes seven beams, the red line arrows and the red circular arrow describe the direction of the polarization vector of these beams, and the angle θ is the incidence angle of each beam relative to z-direction.

3. Reconfigurable HLs and formation of interfaces

From Young's theory of interference, we know that the interference of two plane waves can produce a fringe pattern with a periodicity inversely proportional to the beam incidence angle. So, the angle θ in our multi-beam interference model may also affect the periodicity of the induced lattices. In fact, the relation can be written as $T_h = 2\lambda/(\sqrt{3}n \sin \theta)$ for the horizontal periodicity and $T_v = \lambda/(2n \sin^2(\theta/2))$ for the vertical periodicity (helical pitch) [30]. Thus both the horizontal periodicity and the helical pitch both change with θ at the same time. Since for most of applications, we just want to control the horizontal or vertical cycles, additional control over the interference pattern may be added. Aiming towards this point, let us add a vertical phase $P_z = \pi z/\Lambda$ varying with the propagation direction (along z) to the central beam, where Λ is the longitudinal period. Combing Fig. 2 with Fig. 3, when we add an additional phase term P_z with $\Lambda = 5\lambda$, the pitch changes from $T_v = 107\mu m$ to $T_v = 54\mu m$ while the horizontal periodicity T_h is still kept at $3.9\mu m$ at $\theta=0.02\pi$.

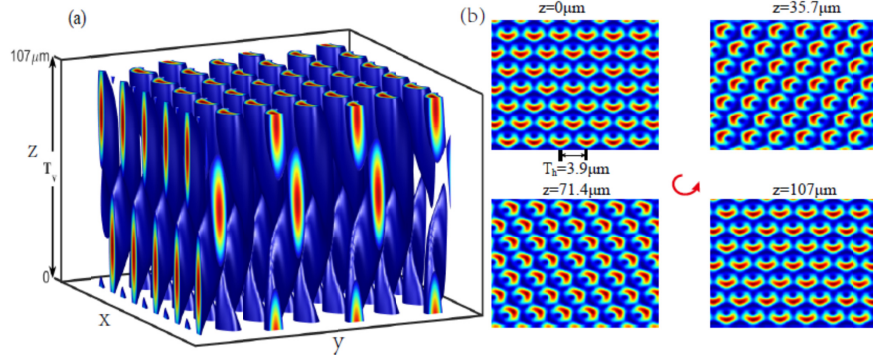


Fig. 2. (a) 3D HL with vertical periodicity (longitudinal periodicity along the propagation z -direction) $T_v = 107\mu\text{m}$ at $\theta=0.02\pi$. (b) Intensity distributions at different z planes. The horizontal periodicity is $T_h = 3.9\mu\text{m}$.

Of course, the pitch varies with Λ while the angle θ is a constant. In practice, to realize this additional phase, we can utilize the transverse-to-longitudinal structuring strategy as established before such as by use of an axicon [41,42], the Pancharatnam-Berry phase element [32], or the spatial light modulator [43].

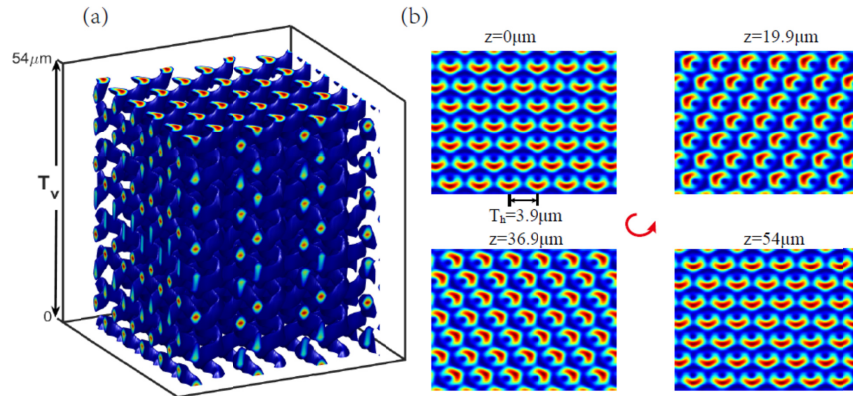


Fig. 3. (a) 3D hexagonal helix lattice with vertical periodicity $T_v = 54\mu\text{m}$ at $\theta=0.02\pi$ by adding an additional phase term P_z to the central beam at $\Lambda = 5\lambda$. (b) Intensity distributions at different z planes. The horizontal periodicity is kept at $T_h = 3.9\mu\text{m}$.

Moreover, we can also add an additional radial (transverse) phase to the central beam to observe the variation of the lattice structure. We start by considering a spiral propagating (blue curve) in free space, as shown in Fig. 4. At any point in time “ s ”, we can draw a line (black line) which is at a tangent to the blue curve. The line is

$$\begin{bmatrix} x \\ y \\ z \end{bmatrix} = \begin{bmatrix} -A\omega\sin(\omega s)(p-s) + A\cos(\omega s) \\ A\omega\cos(\omega s)(p-s) + A\sin(\omega s) \\ p \end{bmatrix}. \quad (2)$$

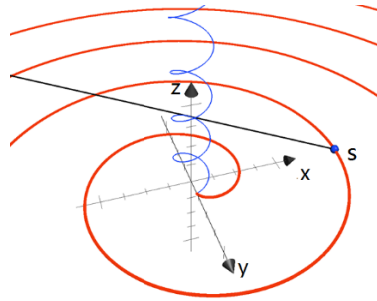


Fig. 4. The formation principle of spiral beams by introducing additional radial phase

This line intersects with the x - y plane when $p = 0$. The spiral amplitude A and the frequency ω can be adjusted as needed. Tracing out the path of the x - y intercept as we vary s with p , we find that the intercept forms an Archimedean spiral (red curve) expressed as Eq. (3). Converting into cylindrical coordinates, we can get the additional radial (transverse) phase P_r as shown in Eq. (4) for angle γ in terms of radius r . Equation (4) can be used to generate such spiral beams.

$$\begin{bmatrix} x \\ y \\ z \end{bmatrix} = \begin{bmatrix} pA\omega\sin(\omega p) + A\cos(\omega p) \\ -pA\omega\cos(\omega p) + A\sin(\omega p) \\ 0 \end{bmatrix}. \quad (3)$$

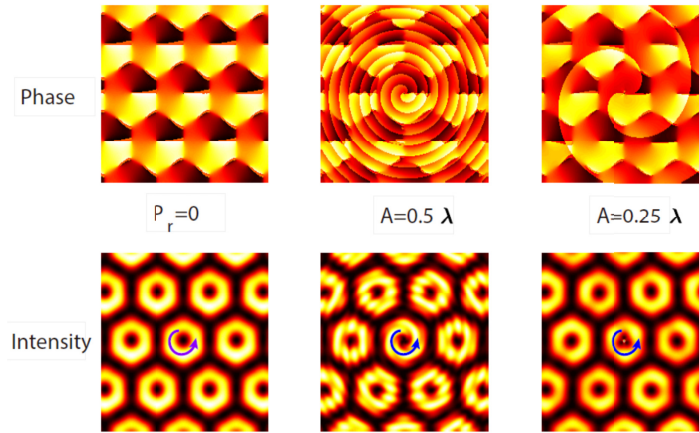


Fig. 5. The phase distributions (top row) and intensity distributions (bottom row) of the HBs at $\theta = 0.01\pi$ and $m = 2$. The left column denotes $P_r = 0$. The middle and right columns denote $A = 0.5\lambda$ and $A = 0.25\lambda$ at $P_r \neq 0$, respectively.

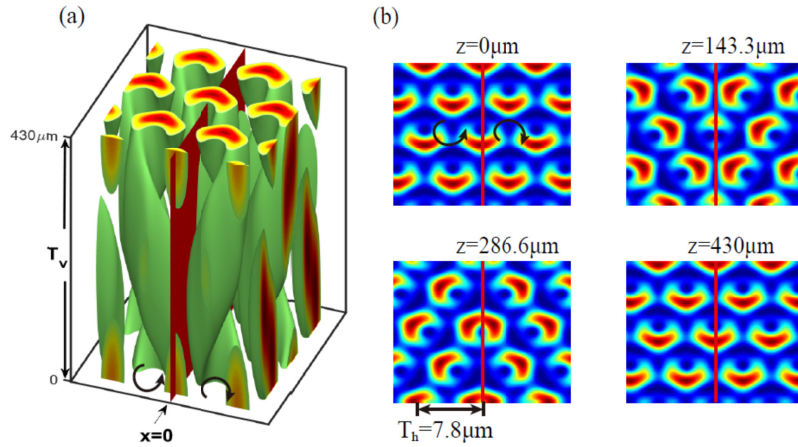


Fig. 6. (a) 3D HL with opposite helicities on both sides of an interface at the $x = 0$ plane at $\theta = 0.01\pi$. (b) Transverse intensity distributions at different z planes. The red line denotes the plane of interface at $x = 0$. Two black curved arrows (in the first two panels) represent the HL with opposite (anticlockwise and clockwise) helicities.

$$P_r = \sqrt{\frac{r^2}{A^2} - 1} + \tan^{-1}\left(-\sqrt{\frac{r^2}{A^2} - 1}\right) - \gamma, \quad (4)$$

where $\gamma = m\varphi$ (m is the topological charge and φ is the azimuth angle). At this point there are a number of ways of creating a spiral beam. We could even make a Laguerre-Bessel beam [44] and impose a spiral rather than a ring-like intensity, which is not the subject of this paper. Here, we only need to add this phase P_r to the central beam for changing the lattice structure. In Fig. 5, we can see that the phase and intensity distributions are different for $P_r = 0$ and $P_r \neq 0$, and they both vary with the spiral amplitude. When we use these beams to induce photonic lattices, we can get different HL structures [12,13,16,26].

Next, we consider to change the phase of the side beams to get an HL which processes opposite helicities on different sides of an interface set at $x = 0$. For the six side beams, the phase is $m\pi/3$ ($m = 0, 1 \dots 5$) at $x \geq 0$. On the contrary, the phase is $-m\pi/3$ ($m = 0, 1 \dots 5$) at $x < 0$. This can be realized by use of spatial light modulators in experiment [23,27]. As shown in Fig. 6, such a lattice structure is realized so that the left ($x < 0$) helicity is anticlockwise, but the right ($x \geq 0$) one is clockwise. Comparing Fig. 2 with Fig. 6, we can further verify that the horizontal periodicity and pitch only vary with the angle θ . When $\theta = 0.01\pi$, we obtain $T_v = 430\mu m$ and $T_h = 7.8\mu m$, and when $\theta = 0.02\pi$, we obtain $T_v = 107\mu m$ and $T_h = 3.9\mu m$. In Fig. 6, though the phase of the side beams varies, the horizontal periodicity and pitch, as defined by $T_h = 2\lambda/(\sqrt{3}n\sin\theta)$ and $T_v = \lambda/(2n\sin^2(\theta/2))$, remain unchanged.

4. Validity of HLs probed by a Gaussian beam

In order to examine the propagation dynamics of an optical beam in the above lattice structures, we first assume that a Gaussian beam, $u(x, y, 0) = 5\exp(-\mu(x^2 + y^2)/\Gamma^2)$ shown in Fig. 7(a), enters the above HL vertically along z -direction, as in an optically induced lattice in a photorefractive crystal, where μ is the beam width factor and $\Gamma = 5\lambda$. Within the approximation of isotropic photorefractive nonlinearity and slowly varying amplitude, the

evolution of an extraordinarily-polarized probe beam u is described by the nonlinear equation with a periodic lattice potential,

$$i \frac{\partial u}{\partial z} + \frac{1}{2k_0 n} \left(\frac{\partial^2 u}{\partial x^2} + \frac{\partial^2 u}{\partial y^2} \right) - \frac{1}{2} k_0 n n_e^3 \gamma_{33} \frac{E_0}{1 + I_L + \sigma |u|^2} u = 0. \quad (5)$$

Here, $k_0 = 2\pi/\lambda$, $n_e = 2.35$ is the refractive index corresponding to e -polarized light in the crystal, $\gamma_{33} = 280 \text{ pm/V}$ is the electro-optic coefficient, and we use $E_0 = 120 \text{ V/mm}$ for the applied electric field. σ is the nonlinearity coefficient, and I_L denotes a HL structure [3,14–18,20–26,30–37]. In Fig. 7(b), one can see that the spatial location of maximum intensity of the probe beam in $y=0$ plane during propagation through the HL at $\theta=0.01\pi$ indeed exhibits a spiral feature. Comparing Fig. 7(c) with Fig. 7(b), we can find that the pitch decreases at $\theta=0.015\pi$. The helix pitch of the probe beam varies accordingly with the helix pitch of the lattice resulting from the change of angle θ . This indicates clearly the spiral waveguide structure has been established in the nonlinear crystal. Interestingly, when the same probe beam enters the lattice interface of opposite helicities of Fig. 6, the beam is divided into two parts which also show opposite helicities, as shown in Fig. 7(d). The pitch of each part is the same as the pitch of the beam in Fig. 7(b) because the incidental angle of the probe beam is the same, that is, $\theta=0.01\pi$. Therefore, it is clear that the incident Gaussian beam follows the spiral path because of the action of the helical waveguides. It is worth noting that such a spirally guided beam is nearly non-diffracting while propagating along the interface. We also note that, from Fig. 7(b) to Fig. 7(d), the nonlinearity coefficient is set at $\sigma=0$, so we only considered the linear propagation and guidance of the probe beam. However, if the nonlinearity ($\sigma \neq 0$) is introduced, the propagation dynamics of the optical beam can be altered in such 3D modulated lattices and interfaces [1–4,8–13,15–17,20]. As an example, we consider such nonlinear propagations of the probe beam in Fig. 7(e) ($\sigma=0.5$) and Fig. 7(f) ($\sigma=1$). Due to self-action of the probe beam itself, we can see that its helix amplitude decreases with the increase of the nonlinearity by comparing Fig. 7(b), Fig. 7(e), and Fig. 7(f). As expected, the introduction of the self-focusing nonlinearity leads to the change of the propagation dynamics of the probe beam through the HL.

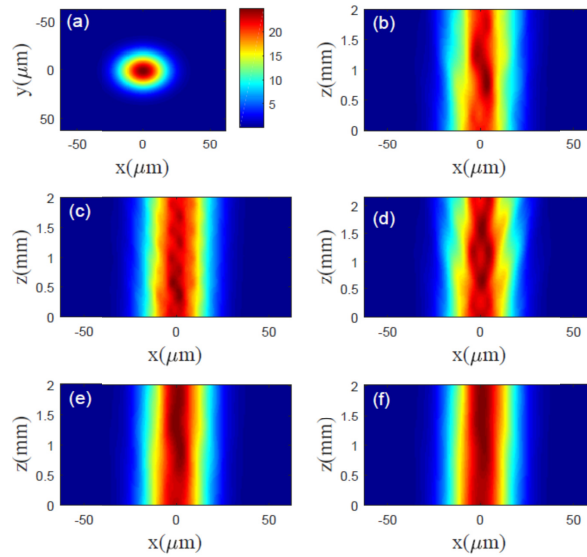


Fig. 7. (a) Input transverse intensity pattern of an incident Gaussian beam with $\mu=0.1$ probing the HL. (b) and (c) are the “side-view” results of the probe beam propagating linearly along the $y = 0$ plane through the bulk HLs (similar to Fig. 2) at $\theta=0.01\pi$ and $\theta=0.015\pi$ for $\sigma=0$, respectively. (d) The propagation of the same probe beam through the HL interface described in Fig. 6 for $\sigma=0$. (e) and (f) are the nonlinear propagation of the same beam through the bulk HL as for (b) but with $\sigma=0.5$ and $\sigma=1$, respectively.

To further examine the spiral feature of optical beams in these HLs, we employ two identical (in-phase) Gaussian beams probing from two opposite sides of the HL interface or domain wall set at the $x = 0$ plane, which can be written as

$$u(x, y, 0) = 5\exp\left(-\mu\left((x-15\times 10^{-6})^2 + y^2\right)/\Gamma^2\right) + 5\exp\left(-\mu\left((x+15\times 10^{-6})^2 + y^2\right)/\Gamma^2\right). \quad (6)$$

Figure 8(a) illustrates this beam with $\mu=0.15$. When the beam enters the lattice interface of same helicities at $\theta=0.015\pi$, one can see that two Gaussian beams first evolve into a somewhat spiral-like structure as that in Fig. 7(c), and their helicity is uniform as seen from Fig. 8(b). However, at a propagation distance of $z > 1\text{mm}$, two beams gradually merge into a single beam due to constructive interference. The inset, which illustrates the beam cross section at the $z = 4\text{mm}$ plane, shows this point more clearly. However, when the width of each probe beam decreases ($\mu=0.2$), the propagation dynamics (Fig. 8(c)) is quite different from the one shown in Fig. 8(b), as each beam tends to follow its own helical waveguide while undergoing the interaction between two beams along the lattice interface. Moreover, when the dipole-like beam in Fig. 8(a) is sent along the HL interface similar to Fig. 6 at $\theta=0.015\pi$, we can see that the two beams follow the spiral path initially with opposite helicities, as shown in Fig. 8(d). When the propagation distance is at $z > 1\text{mm}$, the two beams gradually merge again into a single beam. The difference of helicity between Fig. 8(b) and Fig. 8(d) illustrates well the effect of the HL waveguide structure on the propagation features of the probe beams. We point out that, for Fig. 7 and Fig. 8, we have used beam propagation method [45] to simulate the propagation properties of optical beams. To maintain the required accuracy, we monitor the propagation by calculating the beam power (without taking into account the absorption and scattering) and selecting the optimum choice of step sizes. In addition, the transverse (x and y) window used for simulations is made much wider than the beam width to prevent the beam from hitting the window boundary.

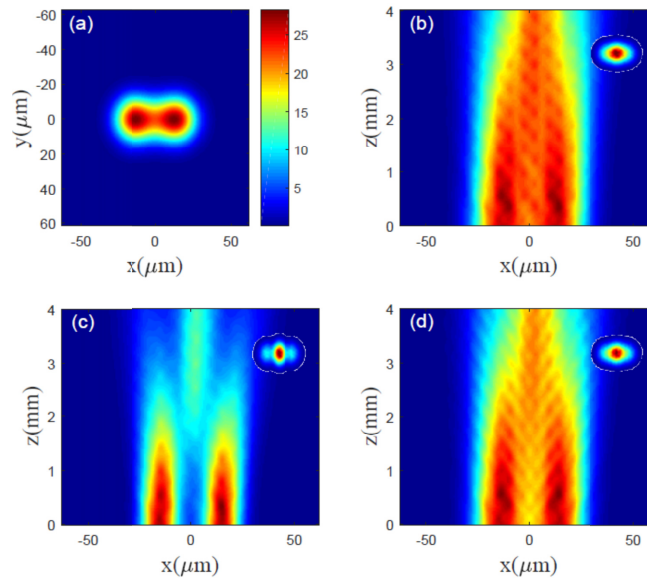


Fig. 8. (a) Intensity pattern of an incident dipole-like beam with $\mu=0.15$ probing the interface. The propagation of the dipole-like beam with $\mu=0.15$ (b) and $\mu=0.2$ (c) in $y = 0$ plane in the HL interface of same helicities. (d) Propagation of the probe beam in (a) in the HL interface of opposite helicities. All insets denote the transverse cross sections of the probe beam at the $z = 4\text{mm}$ plane. The other parameter $\theta=0.015\pi$.

We also point out that, the numerical work presented here has mainly been focused on generation of tunable 3D helical lattices and interfaces, as probed by sending a single or dipole-like Gaussian beam. Linear and nonlinear interface states in such helical lattices certainly merit further theoretical investigations.

5. Conclusions

In conclusion, we have proposed an effective way for generation of complex 3D HLs with tunable helix pitch and spiral direction, as well as such lattices with an interface/domain wall formed by different helicities. Simply by changing the incidence angle of one of the interference beams, the horizontal and vertical periods of the HLs can be varied at ease. To change the vertical period (helix pitch) only, an additional phase of the central beam varying along the propagation direction is introduced, and the change of that phase determines the helix pitch. Moreover, we also contrive a kind of design for HLs with an effective interface having opposite helicity on different sides by introducing different phase structure on the two sides. When an optical beam is sent to probe such HLs and interfaces, it experiences the helicity of the spiraling lattice structures. If the two sides of the effective helical domain wall have opposite helicities, the incident Gaussian or dipole-like probe beam exhibits different propagation dynamics in different sides of the interface. These tunable HLs may be particularly suitable for the studies of fundamental phenomena such as photonic topological surface states and rotation solitons.

Funding

National Key R&D Program of China (Grant No. 2017YFA0303800).

References

1. D. N. Christodoulides, F. Lederer, and Y. Silberberg, "Discretizing light behaviour in linear and nonlinear waveguide lattices," *Nature* **424**(6950), 817–823 (2003).

2. F. Lederer, G. I. Stegeman, D. N. Christodoulides, G. Assanto, M. Segev, and Y. Silberberg, "Discrete solitons in optics," *Phys. Rep.* **463**(1-3), 1–126 (2008).
3. I. L. Garanovich, S. Longhi, A. A. Sukhorukov, and Y. S. Kivshar, "Light propagation and localization in modulated photonic lattices and waveguides," *Phys. Rep.* **518**(1-2), 1–79 (2012).
4. D. H. Song, C. B. Lou, L. Q. Tang, Z. Y. Ye, J. J. Xu, and Z. G. Chen, "Experiments on linear and nonlinear localization of optical vortices in optically induced photonic lattices," *Int. J. Opt.* **2012**, 1 (2012).
5. S. Longhi, M. Marangoni, M. Lobino, R. Ramponi, P. Laporta, E. Cianci, and V. Foglietti, "Observation of dynamic localization in periodically curved waveguide arrays," *Phys. Rev. Lett.* **96**(24), 243901 (2006).
6. S. Longhi and K. Staliunas, "Self-collimation and self-imaging effects in modulated waveguide arrays," *Opt. Commun.* **281**(17), 4343–4347 (2008).
7. A. Szameit, I. L. Garanovich, M. Heinrich, A. A. Sukhorukov, F. Dreisow, T. Pertsch, S. Nolte, A. Tünnermann, and Y. S. Kivshar, "Polychromatic dynamic localization in curved photonic lattices," *Nat. Phys.* **5**(4), 271–275 (2009).
8. Y. V. Kartashov, V. A. Vysloukh, and L. Torner, "Resonant mode oscillations in modulated waveguiding structures," *Phys. Rev. Lett.* **99**(23), 233903 (2007).
9. G. Assanto, L. A. Cisneros, A. A. Minzoni, B. D. Skuse, N. F. Smyth, and A. L. Worthy, "Soliton steering by longitudinal modulation of the nonlinearity in waveguide arrays," *Phys. Rev. Lett.* **104**(5), 053903 (2010).
10. P. Papagiannis, Y. Kominis, and K. Hizanidis, "Power-and momentum-dependent soliton dynamics in lattices with longitudinal modulation," *Phys. Rev. A* **84**(1), 013820 (2011).
11. V. A. Vysloukh, Y. V. Kartashov, and K. Staliunas, "Efficient mode conversion in guiding structures with longitudinal modulation of nonlinearity," *Opt. Lett.* **40**(20), 4631–4634 (2015).
12. M. S. Petrović, "Vortex-induced rotating structures in optical photonic lattices," *Opt. Express* **14**(20), 9415–9420 (2006).
13. D. M. Jović, S. Prvanović, R. D. Jovanović, and M. S. Petrović, "Gaussian-induced rotation in periodic photonic lattices," *Opt. Lett.* **32**(13), 1857–1859 (2007).
14. S. Longhi, "Bloch dynamics of light waves in helical optical waveguide arrays," *Phys. Rev. B* **76**(19), 195119 (2007).
15. Y. V. Kartashov, V. A. Vysloukh, and L. Torner, "Dynamics of topological light states in spiraling structures," *Opt. Lett.* **38**(17), 3414–3417 (2013).
16. A. Zannotti, F. Diebel, M. Boguslawski, and C. Denz, "Chiral light in helically twisted photonic lattices," *Adv. Opt. Mater.* **5**(16), 1–7 (2016).
17. X. Zhang, F. Ye, Y. V. Kartashov, V. A. Vysloukh, and X. Chen, "Localized waves supported by the rotating waveguide array," *Opt. Lett.* **41**(17), 4106–4109 (2016).
18. S. Li, W. Yu, L. Meriggi, Q. Xiao, Z. Nong, X. Cai, M. Sorel, and S. Yu, "High-directional vortex beam emitter based on Archimedean spiral adiabatic waveguides," *Opt. Lett.* **42**(5), 975–978 (2017).
19. L. Lu, J. D. Joannopoulos, and M. Soljačić, "Topological photonics," *Nat. Photonics* **8**(11), 821–829 (2014).
20. M. S. Petrović, A. I. Strinić, N. B. Aleksić, and M. R. Belić, "Rotating solitons supported by a spiral waveguide," *arXiv:1705.08170v1* (2017).
21. M. C. Rechtsman, J. M. Zeuner, Y. Plotnik, Y. Lumer, D. Podolsky, F. Dreisow, S. Nolte, M. Segev, and A. Szameit, "Photonic Floquet topological insulators," *Nature* **496**(7444), 196–200 (2013).
22. Y. Lumer, Y. Plotnik, M. C. Rechtsman, and M. Segev, "Self-localized states in photonic topological insulators," *Phys. Rev. Lett.* **111**(24), 243905 (2013).
23. D. Leykam and Y. D. Chong, "Edge solitons in nonlinear-photonic topological insulators," *Phys. Rev. Lett.* **117**(14), 143901 (2016).
24. D. Leykam, M. C. Rechtsman, and Y. D. Chong, "Anomalous topological phases and unpaired Dirac cones in photonic Floquet topological insulators," *Phys. Rev. Lett.* **117**(1), 013902 (2016).
25. J. Noh, S. Huang, K. P. Chen, and M. C. Rechtsman, "Observation of photonic topological valley Hall edge states," *Phys. Rev. Lett.* **120**(6), 063902 (2018).
26. J. Becker, P. Rose, M. Boguslawski, and C. Denz, "Systematic approach to complex periodic vortex and helix lattices," *Opt. Express* **19**(10), 9848–9862 (2011).
27. M. Padgett, J. Courtial, and L. Allen, "Light's Orbital Angular Momentum," *Phys. Today* **57**(5), 35–40 (2004).
28. T. Latychevskaia and H. W. Fink, "Inverted Gabor holography principle for tailoring arbitrary shaped three-dimensional beams," *Sci. Rep.* **6**(1), 26312 (2016).
29. S. H. Lee, Y. Roichman, and D. G. Grier, "Optical solenoid beams," *Opt. Express* **18**(7), 6988–6993 (2010).
30. M. C. R. Leibovici, "Pattern-Integrated Interference Lithography for Two-Dimensional and Three-Dimensional Periodic-Lattice-Based Microstructures," Ph.D. thesis, School of Electrical and Computer Engineering, Georgia Institute of Technology, Atlanta, Georgia, (2015).
31. G. M. Burrow and T. K. Gaylord, "Multi-Beam interference advances and applications: nano-electronics, photonic crystals, metamaterials, subwavelength structures, optical trapping, and biomedical structures," *Micromachines (Basel)* **2**(2), 221–257 (2011).
32. J. Masajada and B. Dubik, "Optical vortex generation by three plane wave interference," *Opt. Commun.* **198**(1-3), 21–27 (2001).
33. S. Vyas and P. Senthilkumaran, "Interferometric optical vortex array generator," *Appl. Opt.* **46**(15), 2893–2898 (2007).

34. M. Lei, B. Yao, and R. A. Rupp, "Structuring by multi-beam interference using symmetric pyramids," *Opt. Express* **14**(12), 5803–5811 (2006).
35. A. Kapoor, M. Kumar, P. Senthikumar, and J. Joseph, "Optical vortex array in spatially varying lattice," *Opt. Commun.* **365**, 99–102 (2016).
36. X. Li, H. Ma, H. Zhang, Y. Tai, H. Li, M. Tang, J. Wang, J. Tang, and Y. Cai, "Close-packed optical vortex lattices with controllable structures," *Opt. Express* **26**(18), 22965–22975 (2018).
37. Z. Li and C. Cheng, "Generation of second-order vortex arrays with six-pinhole interferometers under plane wave illumination," *Appl. Opt.* **53**(8), 1629–1635 (2014).
38. N. Mitin and A. Pikulin, "Generation of photonic vortex lattices with colloidal monolayers of dielectric microparticles," *Opt. Lett.* **42**(13), 2527–2530 (2017).
39. H. Gao, Y. Li, L. Chen, J. Jin, M. Pu, X. Li, P. Gao, C. Wang, X. Luo, and M. Hong, "Quasi-Talbot effect of orbital angular momentum beams for generation of optical vortex arrays by multiplexing metasurface design," *Nanoscale* **10**(2), 666–671 (2018).
40. J. S. Rodrigues, C. V. C. Mendes, E. J. S. Fonseca, and A. J. Jesus-Silva, "Talbot effect in optical lattices with topological charge," *Opt. Lett.* **42**(19), 3944–3947 (2017).
41. P. Li, Y. Zhang, S. Liu, H. Cheng, L. Han, D. Wu, and J. Zhao, "Generation and self-healing of vector Bessel-Gauss beams with variant state of polarizations upon propagation," *Opt. Express* **25**(5), 5821–5831 (2017).
42. Y. Liu, Y. Ke, J. Zhou, Y. Liu, H. Luo, S. Wen, and D. Fan, "Generation of perfect vortex and vector beams based on Pancharatnam-Berry phase elements," *Sci. Rep.* **7**(1), 44096 (2017).
43. S. Fu, S. Zhang, and C. Gao, "Bessel beams with spatial oscillating polarization," *Sci. Rep.* **6**(1), 30765 (2016).
44. L. Allen, M. W. Beijersbergen, R. J. C. Spreeuw, and J. P. Woerdman, "Orbital angular momentum of light and the transformation of Laguerre-Gaussian laser modes," *Phys. Rev. A* **45**(11), 8185–8189 (1992).
45. O. V. Sinkin, R. Holzlohner, J. Zweck, and C. R. Menyuk, "Optimization of the split-step Fourier method in modeling optical-fiber communications systems," *J. Lightwave Technol.* **21**(1), 61–68 (2003).